Active sites for outer sphere, inner sphere and complex multi-stage electrochemical reactions at polycrystalline boron doped diamond electrodes (pBDD) revealed with scanning electrochemical cell microscopy (SECCM)

*Hollie V. Patten[†], Stanley C.S. Lai[†], Julie V. Macpherson and Patrick R. Unwin**

Department of Chemistry, University of Warwick, Coventry CV4 7AL, United Kingdom

ABSTRACT

The local rate of heterogeneous electron transfer (HET) at polycrystalline boron doped diamond (pBDD) electrodes has been visualized at high spatial resolution for various aqueous electrochemical reactions using scanning electrochemical cell microscopy (SECCM), a technique which uses a mobile pipet-based electrochemical cell as an imaging probe. As exemplar systems, three important classes of electrode reactions have been investigated: outer sphere (one - electron oxidation of ferrocenylmethyltrimethylammonium ($FcTMA^+$)), inner sphere (one - electron oxidation of Fe^{2+}) and complex processes with coupled electron transfer and chemical reactions (oxidation of serotonin). In all cases, the pattern of reactivity is similar: the entire pBDD surface is electroactive, but there are variations in activity between different crystal facets which correlate directly with differences in the local dopant level, as visualized qualitatively by field emission scanning electron microscopy (FE-SEM). No evidence was found for enhanced activity at grain boundaries for any of the reactions. The case of serotonin oxidation is particularly interesting, as this process is known to lead to deterioration of electrodes, due to blocking by reaction products, and so cannot be studied with conventional scanning electrochemical probe microscopy techniques. Yet, we have found this system non-problematic to study because the meniscus of the scanning pipet is only in contact with the surface investigated for a brief time and any blocking product is left behind as the pipet moves to a new location. Thus, SECCM opens up the possibility of investigating and visualizing much more complex heterogeneous electrode reactions than possible presently with other scanning electrochemical probe microscopy techniques.

Introduction

It is now recognized that structural heterogeneities in electrodes impact on the rate of local redox reactions, and that a true understanding of electrochemical reactions requires that spatial variations in electroactivity can be visualized.[1] Thus, techniques that identify microscopic activity and relate this to the corresponding properties of the electrode material are highly valued.[2] In this paper, we demonstrate scanning electrochemical cell microscopy (SECCM),[1d, 3] as a versatile high resolution electrochemical mapping technique, with unique properties that allow it to be used under conditions where other electrochemical imaging techniques would be problematic, for example where rapid surface film formation and electrode blocking occurs.

The focus of our studies is polycrystalline boron doped diamond (pBDD), a well-known example of a heterogeneous electrode which is finding increasing interest for many applications.[4] We show that SECCM provides unambiguous information on electrode surface reactivity, and that the information obtained is far superior to that obtained with previous electrochemical imaging techniques. Knowledge of how electrochemical reactions proceed on different facets of pBDD is important for the optimization of a wide range of possible applications of this material, from sensing to electrocatalysis.[4] Different crystal faces of pBDD incorporate boron to different extents during growth by chemical vapor deposition. For example, the (111) crystal face may incorporate up to ten times more boron than the (100) face during synthesis.[5] This heterogeneity in the local concentration of charge carriers, plus other factors such as the possible presence of sp^2 carbon at grain boundaries,[6] has led to speculation in the literature as to whether the entire surface of pBDD is active or whether there are 'hot spots' of activity.[6-7] To address possible heterogeneities in electrode reaction rates, various flux imaging techniques have been used,

including fluorescence and electrochemiluminescence microscopy[8] and, particularly, scanning electrochemical microscopy (SECM).[6-7] These techniques have highlighted that pBDD electrodes are characterized by spatially heterogeneous electron transfer (HET) rates, but did not have sufficient lateral resolution to resolve individual facets or grain boundaries. Furthermore, a potential drawback of many scanning electrochemical probe microscopy (SEPM) techniques, such as conventional SECM,[2e, 9] and SECM with distance control, as in SECM-AFM,[1f, g, 10] SECM-SICM,[1h, 11] shear force SECM[12] and intermittent contact (IC)-SECM[1c, 13] is that the sample has to be completely immersed in solution. This has three major consequences. First, the spatial resolution depends critically on the electrode size, tip - substrate distance and the kinetics of the process under investigation. The response of SECM methods is thus complicated (to some extent) by diffusional interactions between different reactive regions on the substrate. Consequently, SECM has proven most powerful in situations where the active sites on substrates are displaced a long distance from each other on an otherwise (largely) inert substrate.[1a, 14] Second, imaging with these techniques often requires that the entire electrode substrate is held at under conditions where it is active for the time it takes to record an image (which may typically be tens of minutes to hours). Naturally, this can lead to changes in surface properties over time. Finally, in the worst case, extended immersion (and potential control) of the sample may lead to fouling / deactivation of the substrate (during the course of a scan), making SECM – based techniques very challenging for such studies.

These issues are potentially circumvented if the electrochemical imaging technique involves localized contact of solution with the part of the sample investigated for only a short period. This is one of the key attributes of the SECCM technique which we have recently developed, [2, 14-17]

and which greatly extends the capabilities of earlier microdroplet techniques.[15] SECCM enables electrochemical imaging of surfaces via a borosilicate theta pipet as the electrochemical probe. The theta pipet has two barrels, separated by a glass septum, each of which is filled with the redox electrolyte solution of interest and a quasi-reference counter electrode (QRCE). The pipet (and thus the electrochemical cell) can either be: scanned across the surface, with only the liquid electrolyte droplet at the end of the pipet in contact, to map the surface reactivity, while keeping the tip – substrate separation i.e. meniscus height, constant; or held at a fixed position to perform localized electrochemical experiments such as cyclic voltammetry (CV).

In this paper, we demonstrate the advantages of SECCM in elucidating electrochemical processes at an oxygen – terminated pBDD electrode.[3b, 4d, 7a] In particular, we demonstrate how electrochemical activity of individual facets and grain boundaries on pBDD can be determined readily for different classes of electrode reaction and related to the local surface properties. Among the reactions studied is serotonin oxidation where the electrode is known to foul, making it impossible to study with other electrochemical imaging techniques. Yet, SECCM reveals the heterogeneous activity, and how this relates to the underlying structure, with little impact of the blocking processes.

Experimental

The SECCM set-up has been described recently.[3a, b] In this work, on approach of the pipet tip to the substrate, a 200 mV bias was applied between the QRCEs, giving rise to a mean conductance current (i_{DC}) across the meniscus formed at the mouth of the capillary, whilst a small oscillation (*ca.* 60 nm peak amplitude) was applied to the theta pipet z-position (along the

control axis of the pipet, normal to the substrate). When the meniscus comes into contact with a surface, an alternating current component, i_{AC}, of the conductance current is established, due to the periodic modulation applied to the z-position of the pipet which modulates the meniscus. An i_{AC} set-point is used to obtain the maps and to ensure a constant meniscus height, while scanning across the surface.[3b] This was set between 80-120 pA, approximately 1 % of i_{DC}. The local amperometric current through the pBDD substrate, which is connected as a working electrode, can be measured simultaneously. The substrate is grounded and potential of the solution adjacent to the substrate is controlled by setting the potential of the two QRCEs (while keeping the potential bias between them fixed); the potential the substrate experiences is then typically the midpoint of the potential applied to the two QRCEs, but of opposite sign.[3b] In this way the technique provides local functional information on the (electrochemical) properties of the substrate. Tip positioning is aided with an optical system deployed *in-situ* enabling visualization of the tip relative to the substrate.

The pBDD samples were grown using a commercial microwave plasma - chemical vapor deposition (MW-CVD) process (E6 Ltd., Ascot, U.K.). The average boron doping level of this material is about 5×10^{20} atoms cm^{-3}, as determined by secondary ion mass spectrometry (SIMS)[7a]. The pBDD employed was *ca.* 500 μm thick and an average facet size of 5 – 40 μm. These samples are flat on the scale of SECCM: the roughness is 1 – 2 nm within a facet and 1 - 5 nm between grains, as determined by tapping mode atomic force microscopy (TM-AFM).[4d, 16] Before use, samples were acid cleaned by boiling in concentrated H_2SO_4 (98%), supersaturated with KNO_3 and heated until the KNO_3 had been exhausted.[7a] This treatment results in an oxygen-terminated surface.[17] After acid cleaning, the pBDD sample was rinsed thoroughly with ultra-

pure water, and electrical contact was made to the back of the sample by sputtering (Moorfield Minibox), first Ti (20 nm), followed by Au (400 nm). The sample was then annealed in a tube furnace (Carbolite, UK) at 500°C for 4 hours to create an ohmic titanium carbide contact. The pBDD sample was contacted to a Ti (20 nm) / Au (400 nm) sputter-coated glass slide using Ag paint (Agar Scientific Ltd., UK), and electrical contact was made using tinned copper wire contacted to the slide, again using Ag paint. To correlate measurements with SECCM and field emission - scanning electron microscopy (FE-SEM) (Zeiss Supra 55-VP) in the same area, the sample was marked with a laser-cut cross with lines *ca*. 50 μm wide.[7a] This cross, as well as the grain structure of the sample, could be easily visualized using both the optical system on the SECCM and FE-SEM.

SECCM tips were pulled from borosilicate theta capillaries (TG 150-10, Harvard Part No. 30-0114) using a Sutter P-2000 laser puller (Sutter Instruments, USA), and had an inner diameter of *ca.* 1.5 - 2.5 μm at the end, determined accurately using FE-SEM. This defines the characteristic spatial resolution of SECCM.[1d, 3b] The pulled capillaries were filled with a redox active species and supporting electrolyte of interest using a Microfil needle (WPI Instruments) and syringe. All electrochemical measurements are quoted against silver chloride coated wire (Ag/AgCl) or Pd-H_2 quasi-reference counter electrodes (*vide infra*).

All aqueous solutions were prepared from Milli-Q reagent water (Millipore Corp.) with resistivity 18.2 MΩ cm at 25 °C. The solutions employed in separate experiments were: 2 mM ferrocenylmethyltrimethylammonium ($FcTMA^+$), as the PF_6^- salt prepared in house from $FcTMA^+I^-$ (Strem Chemicals Ltd.) via metathesis with $AgPF_6$ (Strem Chemicals Ltd.) in 50 mM

KCl (Sigma Aldrich); 2 mM iron (II) sulfate ($FeSO_4$) (Sigma-Aldrich) in 0.5 M H_2SO_4 (Sigma Aldrich); and serotonin (5-hydroxytryptamine; Sigma-Aldrich) in 0.1 M NaCl (Sigma Aldrich) and 5 mM HEPES (4-(2-hydroxyethyl)-1-piperazineethanesulfonic acid; Fluka), pH 7.

Results and Discussion

Outer Sphere Electron Transfer

We first consider a classical outer sphere redox mediator, the one-electron oxidation of $FcTMA^+$. Figure 1a shows a typical 50 × 50 μm SECCM image of the pBDD surface for the oxidation of 2 mM $FcTMA^+$ in 50 mM KCl, using a 1.5 μm diameter pipet. The pBDD substrate was held at a potential, E_{sub}, of 300 mV *vs*. Ag/AgCl corresponding to an overpotential, η ($E_{sub} - E^{0'}$) = -8 mV, where $E^{0'}$ is the formal potential. The image was recorded by taking a measurement every 1 μm (itself the average of 1000 points at a sampling rate of 25 kHz, corresponding to 40 ms per measurement). A corresponding field emission - scanning electron micrograph (FE-SEM) of the same area is shown in Figure 1b in which the lighter and darker areas correspond to less-doped and more-doped facets respectively, as confirmed by comparison of FE-SEM with other quantitative techniques, as reported previously.[7a] Comparing the electrochemical activity map obtained using SECCM (Figure 1a) with the FE-SEM image (Figure 1b), it is clear that there is a very close correlation between heterogeneities in the HET rate across the surface (as reflected in the SECCM currents) and the underlying facet properties (as shown in the FE-SEM image). In particular, the high spatial resolution of SECCM shows that there are not only differences between grains but also within single facets. Evidently, areas with higher dopant levels yield a higher current, indicative of faster HET kinetics, illustrating that the local dopant level directly impacts the corresponding local electrochemical reactivity for the case

of outer sphere electron transfer (ET). Furthermore, as only a very small area of the surface is in contact with the solution at every imaging point (much smaller than the typical facet size) the SECCM maps unambiguously show that the entire surface of the pBDD is electrochemically active,[7a, b] with no evidence for any increased intrinsic ET rates at grain boundaries, which has previously been proposed as a possible ET mechanism.[6] Interestingly, there was little detectable difference between CVs recorded on the more and less doped grains, because changes in the voltammetric wave shape are difficult to detect in the fast kinetic regime.[10b] However, kinetic effects are more readily manifested in changes in the current at constant potential highlighting another advantage of the imaging approach at constant potential.[3d]

Based on the observed current, estimates of the standard HET rate constants (k^0) on the different facet types can be made, based on a meniscus diameter of 1.5 μm in this case, a diffusion coefficient $D_{FcTMA} = 6.0 \times 10^{-6}$ cm^2 s^{-1} and a transfer coefficient $\alpha = 0.5$.[3b] Driving the reaction fully (η = 92 mV) under the same experimental conditions, a mass-transport limiting current of 57 pA was found, corresponding to a mass transport coefficient of ~ 0.02 cm s^{-1}. In Figure 1, it can be seen that at η = -8mV the higher dopant areas display a currents of 23.2 ± 1.9 pA (1 σ), not significantly different from the theoretical reversible (Nernstian) current (at this potential) of 24.2 pA. Consequently, in the higher dopant areas, HET is close to reversible under the experimental conditions employed, indicating $k^0 > 0.02$ cm s^{-1}. The lower dopant areas display currents of 16.1 ± 2.0 pA (1 σ), corresponding to an HET rate constant of ~ 0.01 cm s^{-1}, determined by finite element simulations described in detail elsewhere[3b].

Inner Sphere Electron Transfer

We turn to the classical inner sphere redox couple, $Fe^{2+/3+}$.[18] Such HET processes have not been mapped on any electrode surface to the best of our knowledge. The $Fe^{2+/3+}$ redox couple is considered to be sensitive to (the nature of) surface oxygen-containing functional groups on pBDD and carbon electrodes, in general.[18] Because (111) facets are mostly terminated by hydroxyl groups, while the most abundant groups on the (100) facets are ethers or carbonyl groups,[19] this could lead to different interactions of the redox mediator with the surface. Indeed, it has been speculated that the heterogeneous HET kinetics associated with inner-sphere redox couples, such as $Fe^{3+/2+}$, is improved upon oxygen-termination of diamond, due to the catalytic effect of the resulting carbonyl groups.[20]

Figure 2a shows a typical 50 × 50 μm SECCM activity map for the one-electron oxidation of 2 mM Fe^{2+} in 0.5 M H_2SO_4 (pH = 0.3) at a working electrode potential of 1.2 V (versus Pd-H_2, η = 470 mV) obtained using a ~1.5 μm diameter pipet. Similar to the outer sphere redox mediator (Figure 1a), the impact of facet structure of the pBDD (Figure 2a and 2b) on the HET rate is clearly evident in the image, with the more conducting facets again promoting much faster rates of HET. Furthermore, there is again no evidence of enhanced activity at grain boundaries. Note, further, that the difference in electroactivity between the two types of facet is much more distinct than for $FcTMA^{+/2+}$. This difference is especially evident in the CVs recorded by positioning the pipet, with the aid of *in-situ* optical microscopy, on the more and less doped facets (Figure 2c) which show a very clear difference in the onset potential for the oxidation of Fe^{2+} by *ca*. 300 mV. On the other hand, there is no difference in the quartile potential difference, that is the potential difference of currents at ¾ and ¼ of the limiting current value.[21] In both cases $E_{3/4}$-$E_{1/4}$ = 144 ± 2 mV (where i_{lim} was taken at a working electrode potential of 1.2 V in the more conducting region

and 1.4 V in the less conducting region). Such behavior suggests that structural effects of the substrate might be a much more important factor for the reactivity of inner-sphere mediators than for 'classical' outer-sphere mediators.

'Complex' Redox Mediator

Finally, we have employed SECCM to study the oxidation of the neurotransmitter serotonin (5-hydroxytryptamine), a 'complex' electrochemical reaction involving 2 electrons and 2 protons, and complicated further by side reactions.[22] Electrochemistry is widely used as a means of quantitatively measuring serotonin levels in a variety of situations, especially in neurochemistry research, but this is known to be challenging as serotonin oxidation is notorious for rapidly fouling electrode surfaces upon oxidation.[22] Although pBDD is relatively resistant to electrode fouling during serotonin oxidation compared to other carbon electrodes,[23] fouling still occurs, especially under conditions of high mass transport rates. Consequently, conventional electrochemical imaging techniques would be highly problematic for mapping the local reactivity of this process.

We have found that serotonin oxidation rates on pBDD can be imaged successfully to determine local reactivity even though electrode fouling occurs during SECCM mapping. The advantage of SECCM is that only a tiny fraction of the surface is contacted for a brief period by electrolyte solution during a scan, and the blocking product is left in the trail behind as the pipet probe moves to new locations.

Figure 3a highlights the blocking issue, showing sequential CVs of the oxidation of serotonin (0.5 mM in 5 mM HEPES and 0.1 M NaCl) using a 20 μm × 15 μm theta pipet, covering multiple facets, with a 100 mV s^{-1} scan rate. During potential cycling, fouling of the electrode results in a rapid decrease in the limiting current in each cycle, so that after 20 cycles there is essentially no response from the electrode. In contrast, Figure 3b, obtained with a ~2.5 μm diameter pipet, shows a 45 × 45 μm SECCM image for the oxidation of 2 mM serotonin in 5 mM HEPES and 0.1 M NaCl (substrate potential held at 0.65 V *vs.* Ag/AgCl, slightly above the experimental half-wave potential). Significantly, a local reactivity map can be recorded with minimal interference from electrode blocking due to the oxidation process. Furthermore, the current magnitude is 179.2 ± 1.1 pA in the high current regions, a value consistent with expectations for a fast (reversible) two-electron process at this potential and with this size pipet. [3b]Furthermore, it can again be seen that there is strong correlation between the electrochemical activity map and the corresponding facets in the FE-SEM of the same area, shown in Figure 3c. SECCM provides evidence for a clear difference in HET kinetics for the oxidation of serotonin in the different characteristic facets. Again, the distinctive facet structure of pBDD is reflected in the electrochemical image, and there is no enhanced activity at grain boundaries.

The substrate was imaged *in-situ* using the optical microscope of the SECCM positioning system (Figure 3d). This micrograph highlights that during SECCM imaging, serotonin oxidation results in the deposition of an insoluble product on the electrode. Figure 3d shows the film formation after recording one SECCM image (Scan A) and two images at the same location (Scan B & C). It is evident that there is an increase in film thickness with the number of SECCM scans.

We can attribute the success of SECCM in imaging this challenging electrochemical process to the localized and transient nature of the technique, in which the electrode/electrolyte interface is continuously renewed as the pipet is moved during scanning, leaving behind the product. This demonstrates a major advantage of SECCM over conventional electrochemical imaging methods where the substrate would have been immersed in solution and held at conditions where it would be constantly turning over serotonin, leading to rapid electrode fouling.

Conclusions

The considerable capabilities of SECCM as a new electrochemical imaging technique have been demonstrated and new information on HET at pBDD electrodes has been revealed for outer sphere, inner sphere and complex electrochemical reactions (serotonin oxidation). The main conclusions can be summarized as follows. The entire pBDD surface is electrochemically active, but apparent HET rates correlate strongly to facet-dependent boron concentration for all three major classes of reaction. Thus, facets with higher boron content have higher HET activity. For none of the processes studied do we find any evidence for enhanced HET activity at grain boundaries. A particularly exciting feature of SECCM is that it can be employed to visualize redox reactions which foul the electrode surface, providing a powerful advantage over conventional SEPM techniques. The demonstration herein of visualizing serotonin oxidation opens up new possibilities in this arena, particularly of examining complex electrocatalytic reactions on a local scale. In this regard, while SECCM complements SECM-based techniques, it has a clear advantage in the wider range of electrochemical processes it can address.

AUTHOR INFORMATION

Corresponding Author

* corresponding author: p.r.unwin@warwick.ac.uk

Author Contributions

The manuscript was written through contributions of all authors. All authors have given approval to the final version of the manuscript. †These authors contributed equally.

ACKNOWLEDGMENT

We gratefully acknowledge Dr. Michael Snowden for useful discussions and assistance in data analysis, Mr. Neil Ebejer and Dr. Alex Colburn for assistance with the SECCM instrumentation, and Element Six Ltd. for providing us with samples. This work was supported by a Marie Curie Intra European Fellowship within FP7 (project 275450 "VISELCAT") for SCSL and a European Research Council Advanced Investigator Grant (ERC-2009-AdG 247143 "QUANTIF") for PRU.

REFERENCES

(1) (a) Basame, S. B., White, H. S., *J. Phys. Chem.* **1995,** *99,* 16430-16435; (b) Basame, S. B., White, H. S., *Anal. Chem.* **1999,** *71,* 3166-3170; (c) McKelvey, K., Edwards, M. A., Unwin, P. R., *Anal. Chem.* **2010,** *82,* 6334-6337; (d) Ebejer, N., Schnippering, M., Colburn, A. W., Edwards, M. A., Unwin, P. R., *Anal. Chem.* **2010,** *82,* 9141-9145; (e) Shan, X. N., Patel, U., Wang, S. P., Iglesias, R., Tao, N. J., *Science* **2010,** *327,* 1363-1366; (f) Macpherson, J. V., Unwin, P. R., *Anal. Chem.* **2000,** *72,* 276-285; (g) Anne, A., Cambril, E., Chovin, A., Demaille, C., Goyer, C., *ACS Nano* **2009,** *3,* 2927-2940; (h) Takahashi, Y., Shevchuk, A. I., Novak, P., Murakami, Y., Shiku, H., Korchev, Y. E., Matsue, T., *J. Am. Chem. Soc.* **2010,** *132,* 10118-10126; (i) Kim, J., Xiong, H., Hofmann, M., Kong, J., Amemiya, S., *Anal. Chem.* **2010,** *82,* 1605-1607.

(2) (a) Mirkin, M. V., *Mikrochim. Acta* **1999,** *130,* 127-153; (b) Mirkin, M. V., Horrocks, B. R., *Anal. Chim. Acta* **2000,** *406,* 119-146; (c) Edwards, M. A., Martin, S., Whitworth, A. L., Macpherson, J. V., Unwin, P. R., *Physiol. Meas.* **2006,** *27,* R63-R108; (d) Amemiya, S., Bard, A. J., Fan, F. R. F., Mirkin, M. V., Unwin, P. R., *Annu. Rev. Anal. Chem.* **2008,** *1,* 95-131; (e) Bard, A. J., Fan, F. R. F., Kwak, J., Lev, O., *Anal. Chem.* **1989,** *61,* 132-138; (f) Wittstock, G., Burchardt, M., Pust, S. E., Shen, Y., Zhao, C., *Angew. Chem., Int. Ed.* **2007,** *46,* 1584-1617; (g) Bard, A. J., Fan, F. R. F., Pierce, D. T., Unwin, P. R., Wipf, D. O., Zhou, F. M., *Science* **1991,** *254,* 68-74; (h) Mirkin, M. V., Nogala, W., Velmurugan, J., Wang, Y., *Phys. Chem. Chem. Phys.* **2011,** *13,* 21196-21212; (i) Morris, C. A., Friedman, A. K., Baker, L. A., *Analyst* **2010,** *135,* 2190-2202.

(3) (a) Lai, S. C. S., Dudin, P. V., Macpherson, J. V., Unwin, P. R., *J. Am. Chem. Soc.* **2011,** *133,* 10744-10747; (b) Snowden, M. E., Güell, A. G., Lai, S. C. S., McKelvey, K., Ebejer, N.,

O'Connell, M. A., Colburn, A. W., Unwin, P. R., *Anal. Chem.* **2012,** *84,* 2483-2491; (c) Lai, S. C. S., Patel, A. N., McKelvey, K., Unwin, P. R., *Angew. Chem., Int. Ed.* **2012,** doi: 10.1002/201200564; (d) Güell, A. G., Ebejer, N., Snowden, M. E., Macpherson, J. V., Unwin, P. R., *J. Am. Chem. Soc.* **2012,** *134,* 7258-7261.

(4) (a) Salazar-Banda, G. R., Eguiluz, K. I. B., Avaca, L. A., *Electrochem. Commun.* **2007,** *9,* 59-64; (b) Spataru, N., Zhang, X. T., Spataru, T., Tryk, D. A., Fujishima, A., *J. Electrochem. Soc.* **2008,** *155,* B264-B269; (c) Salazar-Banda, G. R., Suffredini, H. B., Avaca, L. A., Machado, S. A. S., *Mater. Chem. Phys.* **2009,** *117,* 434-442; (d) Hutton, L., Newton, M. E., Unwin, P. R., Macpherson, J. V., *Anal. Chem.* **2009,** *81,* 1023-1032.

(5) (a) Janssen, G., van Enckevort, W. J. P., Vollenberg, W., Giling, L. J., *Diamond Relat. Mater.* **1992,** *1,* 789-800; (b) Samlenski, R., Haug, C., Brenn, R., Wild, C., Locher, R., Koidl, P., *Diamond Relat. Mater.* **1996,** *5,* 947-951; (c) Spitsyn, B. V., Bouilov, L. L., Derjaguin, B. V., *J. Cryst. Growth* **1981,** *52,* 219-226.

(6) Holt, K. B., Bard, A. J., Show, Y., Swain, G. M., *J. Phys. Chem. B* **2004,** *108,* 15117-15127.

(7) (a) Wilson, N. R., Clewes, S. L., Newton, M. E., Unwin, P. R., Macpherson, J. V., *J. Phys. Chem. B* **2006,** *110,* 5639-5646; (b) Neufeld, A., O'Mullane, A., *J. Solid State Electrochem.* **2006,** *10,* 808-816; (c) Wang, S., Swain, G. M., *J. Phys. Chem. C* **2007,** *111,* 3986-3995.

(8) (a) Colley, A. L., Williams, C. G., Johansson, U. D., Newton, M. E., Unwin, P. R., Wilson, N. R., Macpherson, J. V., *Anal. Chem.* **2006,** *78,* 2539-2548; (b) Chiku, M., Nakamura, J., Fujishima, A., Einaga, Y., *Anal. Chem.* **2008,** *80,* 5783-5787.

(9) (a) Kwak, J., Bard, A. J., *Anal. Chem.* **1989,** *61,* 1221-1227; (b) Kwak, J., Bard, A. J., *Anal. Chem.* **1989,** *61,* 1794-1799.

(10) (a) Dobson, P. S., Weaver, J. M. R., Holder, M. N., Unwin, P. R., Macpherson, J. V., *Anal. Chem.* **2005,** *77,* 424-434; (b) Mirkin, M. V., Bard, A. J., *Anal. Chem.* **1992,** *64,* 2293-2302; (c) Smirnov, W., Kriele, A., Hoffmann, R., Sillero, E., Hees, J., Williams, O. A., Yang, N., Kranz, C., Nebel, C. E., *Anal. Chem.* **2011,** *83,* 4936-4941.

(11) Takahashi, Y., Shevchuk, A. I., Novak, P., Zhang, Y. J., Ebejer, N., Macpherson, J. V., Unwin, P. R., Pollard, A. J., Roy, D., Clifford, C. A., Shiku, H., Matsue, T., Klenerman, D., Korchev, Y. E., *Angew. Chem.-Int. Edit.* **2011,** *50,* 9638-9642.

(12) (a) Ballesteros Katemann, B., Schulte, A., Schuhmann, W., *Chem. Eur. J.* **2003,** *9,* 2025-2033; (b) Hengstenberg, A., Kranz, C., Schuhmann, W., *Chem. Eur. J.* **2000,** *6,* 1547-1554.

(13) McKelvey, K., Snowden, M. E., Peruffo, M., Unwin, P. R., *Anal. Chem.* **2011,** *83,* 6447-6454.

(14) (a) Serebrennikova, I., White, H. S., *Electrochem. Solid-State Lett.* **2001,** *4,* B4-B6; (b) Ye, H., Park, H. S., Bard, A. J., *J. Phys. Chem. C* **2011,** *115,* 12464-12470; (c) Ballesteros Katemann, B., Schulte, A., Schuhmann, W., *Electroanal.* **2004,** *16,* 60-65; (d) Sa, N., Baker, L. A., *J. Am. Chem. Soc.* **2011,** *133,* 10398-10401; (e) Ishimatsu, R., Kim, J., Jing, P., Striemer, C. C., Fang, D. Z., Fauchet, P. M., McGrath, J. L., Amemiya, S., *Anal. Chem.* **2010,** *82,* 7127-7134.

(15) (a) Williams, D. E., Mohiuddin, T. F., Zhu, Y. Y., *J. Electrochem. Soc.* **1998,** *145,* 2664-2672; (b) Spaine, T. W., Baur, J. E., *Anal. Chem.* **2001,** *73,* 930-938; (c) Lohrengel, M. M., Moehring, A., Pilaski, M., *Fresenius' J. Anal. Chem.* **2000,** *367,* 334-339; (d) Suter, T., Böhni, H., *Electrochim. Acta* **1997,** *42,* 3275-3280; (e) Suter, T., Böhni, H., *Electrochim. Acta* **2001,** *47,*

191-199; (f) Williams, C. G., Edwards, M. A., Colley, A. L., Macpherson, J. V., Unwin, P. R., *Anal. Chem.* **2009,** *81,* 2486-2495.

(16) Hutton, L. A., Newton, M. E., Unwin, P. R., Macpherson, J. V., *Anal. Chem.* **2011,** *83,* 735-745.

(17) (a) Pehrsson, P. E., Long, J. P., Marchywka, M. J., Butler, J. E., *Appl. Phys. Lett.* **1995,** *67,* 3414-3416; (b) Liu, F. B., Wang, J. D., Liu, B., Li, X. M., Chen, D. R., *Diamond Relat. Mater.* **2007,** *16,* 454-460.

(18) Chen, P., McCreery, R. L., *Anal. Chem.* **1996,** *68,* 3958-3965.

(19) (a) Thomas, R. E., Rudder, R. A., Markunas, R. J., *J. Vac. Sci. Technol., A* **1992,** *10,* 2451-2457; (b) Nebel, C. E., Ristein, J., *Thin-Film Diamond II*. Elsevier Academic Press: 2004.

(20) Fischer, A. E., Show, Y., Swain, G. M., *Anal. Chem.* **2004,** *76,* 2553-2560.

(21) Bard, A., Faulkner, L. R., *Electrochemical Methods: Fundamentals and Applications, 2nd Edition* **2001**.

(22) (a) Sarada, B. V., Rao, T. N., Tryk, D. A., Fujishima, A., *Anal. Chem.* **2000,** *72,* 1632-1638; (b) Wrona, M. Z., Dryhurst, G., *J. Org. Chem.* **1987,** *52,* 2817-2825; (c) Wrona, M. Z., Dryhurst, G., *J. Electroanal. Chem. Interfacial Electrochem.* **1990,** *278,* 249-267.

(23) Güell, A. G., Meadows, K. E., Unwin, P. R., Macpherson, J. V., *Phys. Chem. Chem. Phys.* **2010,** *12,* 10108-10114.

Figure 1

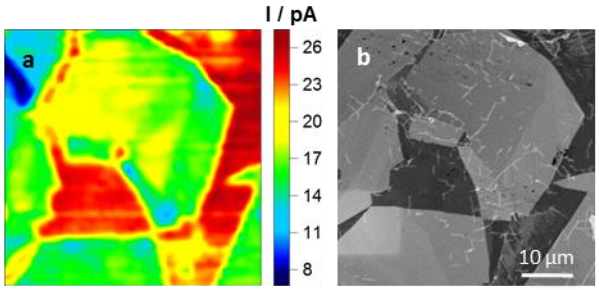

Figure 1. a) 50 × 50 µm SECCM image showing the oxidation of 2 mM $FcTMA^+$ in 50 mM KCl at 300 mV *vs.* Ag/AgCl (η = - 8mV). b) Corresponding FE-SEM image of the same area.

Figure 2

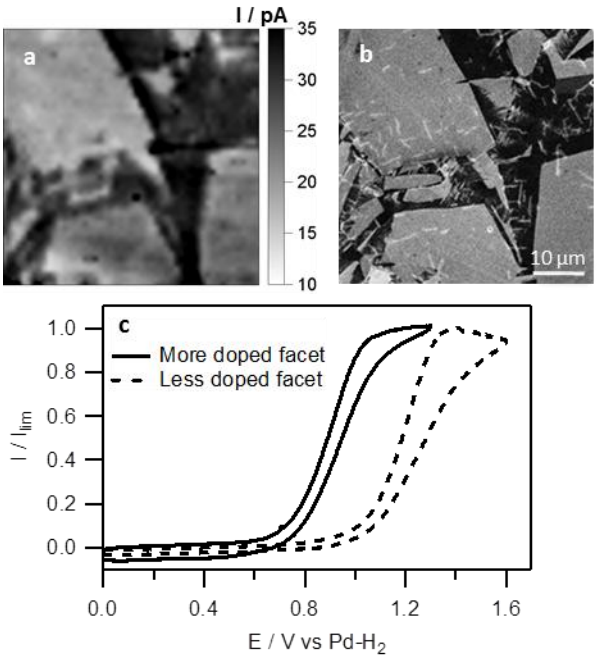

Figure 2. a) 50 × 50 µm SECCM image of the oxidation of 2 mM Fe^{2+} in 0.5 M H_2SO_4 at 1.2 V *vs.* Pd-H_2 (η = 470 mV). b) Corresponding FE-SEM image of the same area. c) CVs recorded on a more and less boron doped facet at a scan rate of 100 mV s^{-1}.

Figure 3

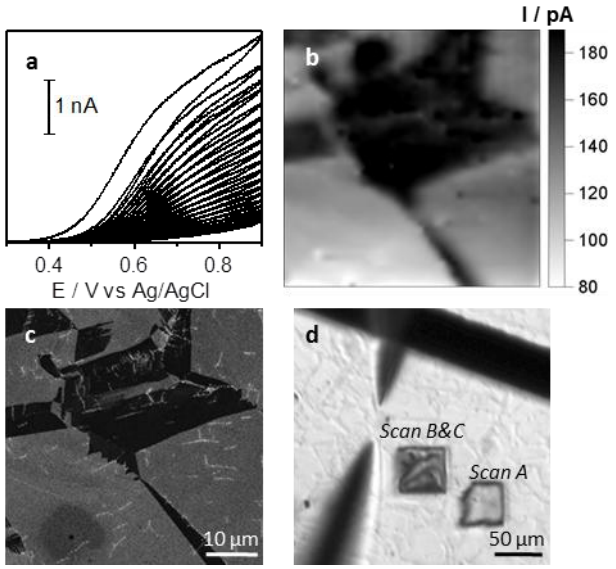

Figure 3. a) CVs for the oxidation of 2 mM serotonin in 5 mM HEPES and 0.1 M NaCl at a scan rate of 100 mV s^{-1} using a 20 µm × 15 µm capillary. b) 45 × 45 µm SECCM image showing the oxidation of 2 mM serotonin at 650 mV *vs.* Ag/AgCl. A clear effect of facet structure is observed. c) Corresponding FE-SEM image of the same area. d) SECCM camera image of the pBDD substrate after recording SECCM images. Film formation can be observed after recording one SECCM image (labeled 'scan A') and after two images recorded over the same area (labeled 'scan B & C'). Also visible are the pipet and its reflection on the surface, the grain structure of the pBDD surface, and a laser-cut line.

TOC Image

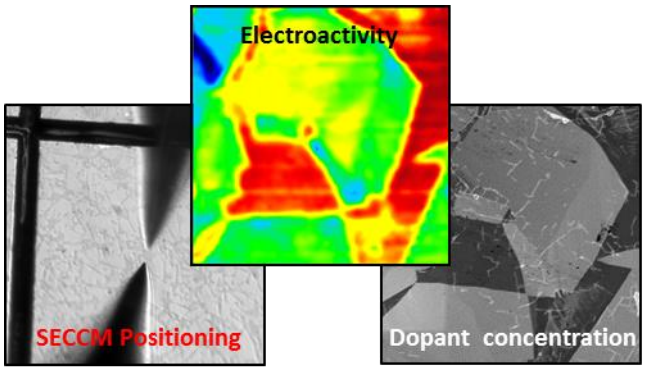
Electroactivity
SECCM Positioning
Dopant concentration